Preprints.org

Article

Not peer-reviewed version

Quantum Control of Metrological Quantities in Two-Component Bose–Einstein Condensates

Henan Wang , Qimeng Zhang , Hengyan Wang , Hai-Jun Xing * , Yixiao Huang *

Posted Date: 31 March 2026

doi: 10.20944/preprints202603.2482.v1

Keywords: quantum metrology; Bose-Einstein condensates; collective spin; Dicke basis; quantum Fisher information; Shannon entropy

Article

Quantum Control of Metrological Quantities in Two-Component Bose–Einstein Condensates

Henan Wang [1], Qimeng Zhang [1], Hengyan Wang [1], Hai-Jun Xing [2,*] and Yixiao Huang [1,*]

1 School of Science, Zhejiang University of Science and Technology, Hangzhou 310023, China
2 Center for Quantum Sciences and School of Physics, Northeast Normal University, Changchun 130024, China
* Correspondence: hjxing@nenu.edu.cn (H.-J.X.); yxhuang@zust.edu.cn (Y.-X.H.)

Abstract

We investigate a two-component Bose-Einstein condensate as a platform for quantum metrology and characterize the dynamical evolution of the quantum state using two complementary metrics: the quantum Fisher information and the normalized Shannon entropy. With time-dependent control, metrological resources can be prepared and stabilized over a finite time window. These schemes provide a comprehensive assessment of the quantum dynamics in terms of phase sensitivity and the concentration of the state distribution, thereby offering a theoretical basis for designing robust quantum metrology protocols.

Keywords: quantum metrology; Bose-Einstein condensates; collective spin; Dicke basis; quantum Fisher information; Shannon entropy

---

1. Introduction

High-precision parameter estimation is critical for both theoretical and experimental studies. The quantum parameter estimation theory indicates that the precision can be substantially increased via utilizing quantum resources such as quantum entanglement and squeezing [1–8]. The demands for creating and manipulating these resources highlight systems such as the Bose-Einstein condensates (BEC) [9–14], which we focus on in this manuscript. Under the two-mode approximation, a two-component BEC can be mapped to a collective spin model [15]. For fixed total particle number N, the collective-spin description is confined to the totally symmetric subspace with $j = N/2$ [16]. Its dynamic is jointly governed by the collision-induced one-axis-twisting (OAT) [5,17,18] term $\hat{J}_z^2$ and the Josephson-type linear coupling [19–21] $\hat{J}_x$ generated by radio frequency or microwave driving. Previous studies have shown that, for suitable coupling strengths and evolution times, this dynamics can markedly improve quantum sensitivity [22–25].

The quantum Fisher information (QFI) serves as a primary precision measure in the quantum parameter estimation framework. It upper bounds the achievable estimation precision through the quantum Cramér–Rao inequality [1,2]. In addition, the probability distribution of a many-body state in the Dicke basis [26] is crucial for understanding its dynamical features, and the Shannon entropy [27] provides a compact scalar measure of how concentrated this distribution is. In the present context, analyzing these two metrics in parallel enables a direct and quantitative characterization of the high phase sensitivity and the localization of the evolving state in the Dicke basis. Although these metrics have been widely used in studies of quantum metrology [7,10,28,29], a systematic examination of their respective roles within the same framework remains relatively underexplored.

Motivated by the above considerations, we introduce a scheme for manipulating the two metrological resources within the framework of a two-component BEC system. We begin by investigating the temporal structures of these two metrics under the free evolution, which is generated by a combination of a constant transverse field and spin-squeezing interaction. Building on the analysis, we introduce a control protocol in which the transverse field is switched off either at the QFI peak or at the entropy

 doi:10.20944/preprints202603.2482.v1

minimum. Numerical results demonstrate a universal effect: applying the control at the optimal time can generate stable plateaus in the target quantity. This provides a theoretical framework for generating and preserving metrological resources, which is advantageous for realizing a time-robust quantum metrology scheme in the two-component condensates.

This manuscript is arranged as follows. In Sec. 2, we detail the two-mode BEC system. Sec. 3 introduces the normalized QFI, whose dynamics and control scheme are given in Sec. 4. Sec. 5 introduces the normalized Shannon entropy, whose dynamics and control scheme are given in Sec. 6. Finally, we conclude in Sec. 7.

2. Model

We consider a weakly interacting two-component Bose-Einstein condensate tightly confined in an external trapping potential. The condensates are composed of N Bosons with two internal hyperfine states $|a\rangle$ and $|b\rangle$, which are coherently coupled via a radio frequency or microwave field. Under the two-mode approximation, the effective collective-spin Hamiltonian takes the form [18]

$$\hat{H}(t) = 2\kappa\hat{J}_z^2 + \Omega(t)\hat{J}_x, \tag{1}$$

where $\hat{J}_x = \frac{1}{2}(\hat{a}^\dagger\hat{b} + \hat{b}^\dagger\hat{a})$, $\hat{J}_z = \frac{1}{2}(\hat{b}^\dagger\hat{b} - \hat{a}^\dagger\hat{a})$, together with $\hat{J}_y = \frac{1}{2i}(\hat{a}^\dagger\hat{b} - \hat{b}^\dagger\hat{a})$ denote the collective-spin operators in the Schwinger representation, with the total spin length $j = N/2$. Accordingly, the following analysis is carried out within this totally symmetric subspace. Here, $\hat{a}$ ($\hat{a}^\dagger$) and $\hat{b}$ ($\hat{b}^\dagger$) are the mode annihilation (creation) operators for atoms in the internal states $|a\rangle$ and $|b\rangle$, respectively.

Specifically, the first OAT term $2\kappa\hat{J}_z^2$ in $\hat{H}(t)$ originates from two-body s-wave collisional interactions. The coefficient can be acquired under: i) the single spatial mode approximation $\hat{\Psi}_\alpha(\mathbf{r}) \simeq \phi(\mathbf{r})\hat{a}_\alpha$ [30–32] valid in strong confinement and low temperature, and ii) conservation of the total particle number $\hat{N} = \hat{n}_a + \hat{n}_b$. The remaining nonlinear coefficient reads $\kappa \propto (\kappa_{aa} + \kappa_{bb} - 2\kappa_{ab})$ [33,34]. Here, $\kappa_{\alpha\beta}$ denotes the spin-dependent interaction strength, which can be tuned via the Feshbach resonance [35].

The second Josephson-type term $\Omega(t)\hat{J}_x$ in $\hat{H}(t)$ originates in the coherent coupling between the two internal states, which is induced by a radio frequency or microwave field that is near-resonant with the transition $|a\rangle \leftrightarrow |b\rangle$. The atom–field interaction contributes this term under the rotating-wave approximation and the single spatial-mode approximation. The coefficient $\Omega(t)$ illustrates the effective Rabi frequency, which can be time-modulated via the field amplitude and pulse shape.

3. Quantum Fisher Information

The QFI quantifies the sensitivity of a parameterized quantum state $|\psi_\phi\rangle$ to an unknown parameter ϕ. It lower bounds the variance of a unbiased estimator ϕ_{est} via the quantum Cramér–Rao inequality, which states [1,2]

$$\Delta^2\phi \geq \frac{1}{\nu F_Q}. \tag{2}$$

Here, ν is the repetition, F_Q is the QFI, which will be detailed below. This indicates that the QFI quantifies the ultimate precision achievable in a parameter estimation scheme, thus serving as a primary measure in quantum metrology.

In the scenario considered in this manuscript, we set the system to remain in a pure state $|\psi(t)\rangle$ throughout the evolution. The parameter ϕ is introduced via an unitary encoding process $|\psi_\phi\rangle = e^{-i\phi\hat{G}}|\psi(t)\rangle$, which is generated by an operator $\hat{G}$. For such a process, the QFI is simply four times the generator's variance [36],

$$F_Q[|\psi(t)\rangle, \hat{G}] = 4\,\Delta\hat{G}^2(t) = 4(\langle\hat{G}^2\rangle_t - \langle\hat{G}\rangle_t^2), \tag{3}$$

where $\Delta\hat{G}^2(t)$ denotes the variance of $\hat{G}$ in the state $|\psi(t)\rangle$, with $\langle\cdot\rangle \equiv \langle\psi(t)|\cdot|\psi(t)\rangle$.

In this manuscript, we focus on the QFI associated with state $|\psi(t)\rangle$ under spin rotations about an arbitrary direction $\boldsymbol{n} = (n_x, n_y, n_z)^{\mathrm{T}}$ within the collective-spin representation. Here, the generator $\hat{G}$ is denoted as $\hat{J}_{\boldsymbol{n}} = \sum_{i=x,y,x} n_i \hat{J}_i$, and its variance can be formalized as the quadratic form

$$\Delta \hat{J}_{\boldsymbol{n}}^2(t) = \boldsymbol{n}^{\mathrm{T}} \boldsymbol{\Gamma}(t)\, \boldsymbol{n}, \tag{4}$$

where $\boldsymbol{\Gamma}(t)$ is a three-dimensional covariance matrix defined as $\Gamma_{ij}(t) = \frac{1}{2}\langle \hat{J}_i\hat{J}_j + \hat{J}_j\hat{J}_i\rangle_t - \langle \hat{J}_i\rangle_t\langle \hat{J}_j\rangle_t$ with $i, j \in \{x, y, z\}$. We further denote the maximum variance among all directions $\boldsymbol{n}$ with $\lambda_{\max}\Delta \hat{J}_{\boldsymbol{n}}^2(t)$, which corresponds to the largest eigenvalue of $\boldsymbol{\Gamma}(t)$. The maximal QFI acquired for states at time t then reads $F_Q^{\max}(t) = 4\,\lambda_{\max}\Delta \hat{J}_{\boldsymbol{n}}^2(t)$. For convenience, we introduce the normalized QFI (nQFI)

$$\bar{F}_Q = \frac{F_Q^{\max}(t)}{N} = \frac{4}{N}\,\lambda_{\max}\Delta \hat{J}_{\boldsymbol{n}}^2(t) \tag{5}$$

for the collective-spin system with particle number $N = 2j$. We will take it as the main metric to quantify the metrological capability at different stages of the evolution.

4. Quantum Dynamics of Quantum Fisher Information

In this section, we focus on the dynamics generated by the effective Hamiltonian $\hat{H}(t)$ given by Eq. (1) and investigate its effect on the QFI.

We begin by preparing the condensates into the spin coherent state pointing in (θ_0, ϕ_0) direction, i.e.,

$$|\psi(0)\rangle = |\theta_0, \phi_0\rangle_{\mathrm{SCS}} \equiv e^{-i\phi_0 \hat{J}_z} e^{-i\theta_0 \hat{J}_y} |j, j\rangle, \tag{6}$$

where $|j, j\rangle$ is the eigen-state of $\hat{J}_z$ with maximal eigenvalue with $j = N/2$. Furthermore, we choose $(\theta_0, \phi_0) = (\pi/2, 0)$ in the following discussions, so that all of the atom spins point along the x direction initially. Then, we subject this state to a two-stage dynamical evolution as detailed below.

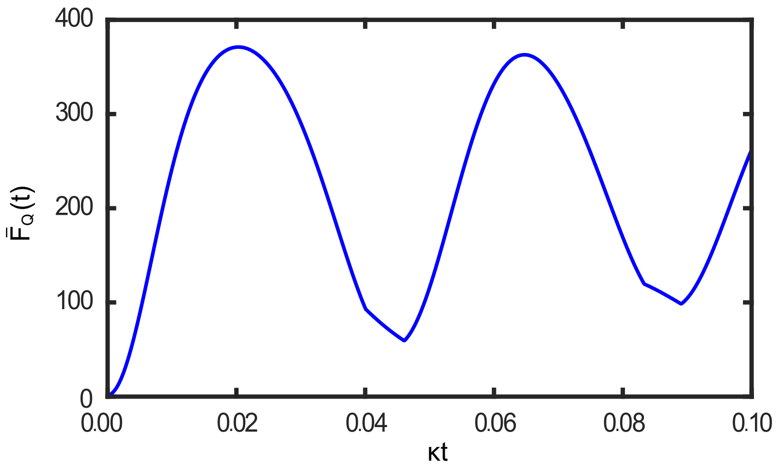

Figure 1. Free evolution of $\bar{F}_Q(t)$ under a constant transverse field. The total particle number is $N = 1000$. The results correspond to the coupling ratio $\Omega_R/\kappa = 3$.

Firstly, we focus on the Hamiltonian Eq. (1) with a constant transverse field $\Omega(t) = \Omega_R$, where the states evolves as

$$|\psi(t)\rangle = e^{-i\hat{H}_1 t}|\psi(0)\rangle, \tag{7}$$

with

$$\hat{H}_1(t) = 2\kappa \hat{J}_z^2 + \Omega_R \hat{J}_x \tag{8}$$

in this evolution. Here, the nonlinear term $2\kappa\hat{J}_z^2$ produces a shearing of the collective-spin distribution, whereas the linear coupling $\Omega_R \hat{J}_x$ induces coherent mixing between the two internal components $\hat{a}$

 doi:10.20944/preprints202603.2482.v1

and $\hat{b}$. These contributions jointly drive the system away from the coherent state toward a non-classical many-body state with enhanced metrological sensitivity.

As illustrated in Fig. 1, under the free evolution (Eq. (7)), the nQFI $\bar{F}_Q(t)$ along the optimal direction typically displays a primary-peak-and-oscillation pattern, where the first local maximum is attained at $t = t_F$. At early times ($t < t_F$), $\bar{F}_Q(t)$ increases in an approximately monotonic manner, rising within a short time from the standard-quantum-limit level of a coherent state to values well above unity. This enhancement can be attributed to the shearing action of OAT dynamics on the Bloch sphere: quantum fluctuations are squeezed along an optimal direction and stretched along the orthogonal direction, thereby increasing the variance along the optimal generator direction and, consequently, the QFI. This early-time behavior is consistent with established results on spin squeezing and the generation of non-classical correlations in OAT models, indicating that the Hamiltonian Eq. (1) can yield substantial metrological gain under the free evolution.

At later times ($t > t_F$), the amplitude distribution of $|\psi(t)\rangle$ in the $\hat{J}_z$ eigenbasis becomes progressively over-sheared, which results in strongly nonuniform relative phases among different magnetic-sublevel components and gives rise to intricate interference patterns on the Bloch sphere. Although the state remains highly nonclassical, the phase-sensitive optimal direction in the three-dimensional spin space varies rapidly with time, and the maximal variance extracted from the covariance matrix does not remain close to its early-time peak value. As a result, $\bar{F}_Q(t)$ exhibits a pronounced collapse after the primary peak, followed by secondary peaks and oscillations. Such a peak–collapse–partial-revival temporal profile is a typical manifestation of quasi-periodic many-body quantum interference in finite-dimensional systems. In the specific case of $\Omega_R/\kappa = 3$, the interplay between nonlinear twisting and transverse coupling results in the characteristic quasi-periodic behavior observed in Fig. 1.

Building on the above free evolution, we propose a time-control protocol to reduce sensitivity to the precise evolution time and to sustain a high, approximately constant QFI over a finite time window. Specifically, we rapidly switched off the transverse field at the time t_F when $\bar{F}_Q(t)$ first attains a local maximum under free evolution, so that the Hamiltonian reads

$$\hat{H}_2(t) = \begin{cases} 2\kappa\hat{J}_z^2 + \Omega_R\hat{J}_x, & 0 \le t < t_F \\ 2\kappa\hat{J}_z^2, & t_F \le t. \end{cases} \tag{9}$$

In the interval $0 \le t < t_F$, the interplay between the nonlinear term $2\kappa\hat{J}_z^2$ and the transverse coupling $\Omega_R\hat{J}_x$ generates strong non-classical correlations and increases $\bar{F}_Q(t)$ to values far above unity near the primary peak as demonstrated by Fig. 2. Around t_F, we find that the optimal generator direction extracted from the covariance matrix typically lies close to the z axis. This can be understood from the fact that the twisting term reduces the minimum fluctuation, generating a squeezed state, while the transverse coupling rotates the state such that the direction of minimum fluctuation aligns near the z axis. After the switch-off of Ω at $t = t_F$, the further mixing and interference induced by $\hat{J}_x$ is absent, leaving the state predominantly accumulated phases in the $\hat{J}_z$ eigen-basis. Correspondingly, the QFI does not exhibit a pronounced collapse but instead forms a relatively flat plateau close to the peak value.

To further demonstrate the robustness of the protocol, we apply this free-evolution–switch-off scheme to various coupling ratios Ω_R/κ, yielding the results shown in Fig. 2. As illustrated, the dashed curves correspond to free evolution generated by $\hat{H}_1$, characterized by a rapid rise to the primary peak followed by collapse and oscillations, whereas the solid curves show the evolution after switching off the transverse coupling at the corresponding time t_F. For $t \ge t_F$, the solid curves no longer display a pronounced collapse and revival; instead, they exhibit a plateau of appreciable duration near the peak height with only weak residual variations. This latching behavior substantially extends the usable time window associated with high QFI. Moreover, upon optimizing the coupling ratio, the post-switch-off plateau height exhibits Heisenberg scaling, namely $\bar{F}_Q(t) \simeq N/2$, or equivalently $F_Q^{\max}(t) \simeq N^2/2$.

Preprints.org (www.preprints.org) | NOT PEER-REVIEWED | Posted: 31 March 2026 doi:10.20944/preprints202603.2482.v1

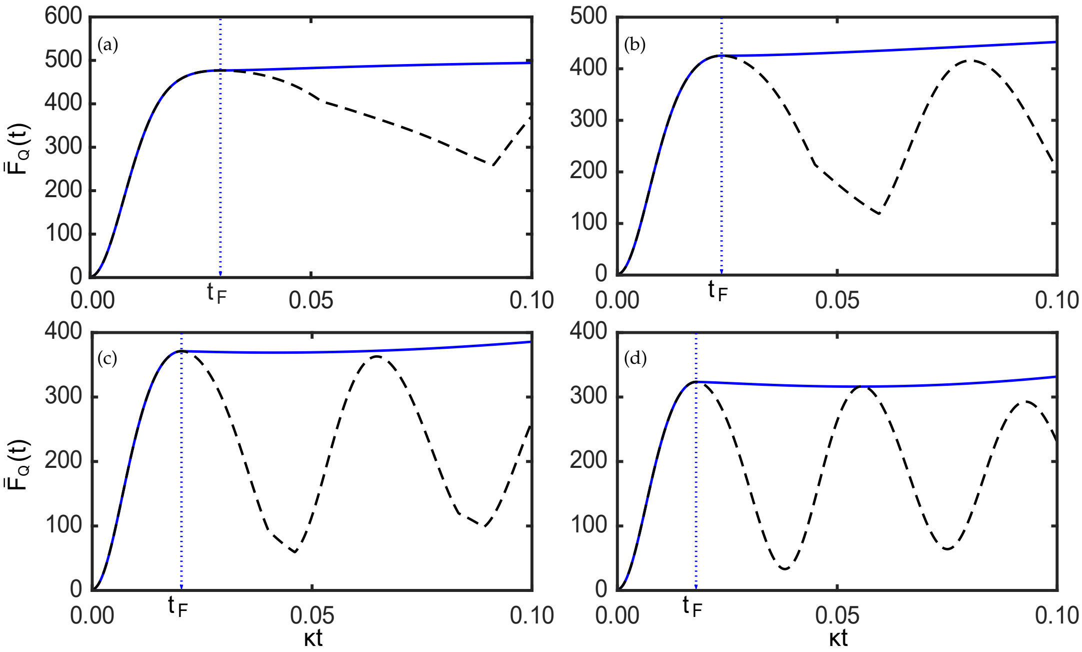

Figure 2. Latching behavior of the quantum Fisher information. The total particle number is $N = 1000$. The four panels correspond to (a) $\Omega_R/\kappa = 1$, (b) $\Omega_R/\kappa = 2$, (c) $\Omega_R/\kappa = 3$, and (d) $\Omega_R/\kappa = 4$. The dashed curves show the free-evolution $\bar{F}_Q(t)$. The solid curves show the evolution after switching off the transverse coupling at t_F.

5. Normalized Shannon Entropy

Entropy-based measures provide a concise way to characterize how broadly the evolving many-body state is distributed in a chosen basis. For two-mode pure states, a widely used quantitative measure is the entanglement entropy [37], i.e., the von Neumann entropy of the reduced density matrix obtained by tracing out a subsystem. For the two-component BEC described above, it is natural to make the bi-partition between the two internal states (modes), namely $a|b$. Specifically, we expand the pure state $|\psi(t)\rangle$ in the Dicke basis of the collective spin as

$$|\psi(t)\rangle = \sum_{m=-j}^{j} c_m(t)\,|j,m\rangle = \sum_{m=-j}^{j} c_m(t)\,|j+m\rangle_a|j-m\rangle_b, \tag{10}$$

where the last equality is acquired by mapping $|j,m\rangle$ to the two-mode Fock state $|n_a\rangle_a|n_b\rangle_b$ via $n_a = j+m$, $n_b = j-m$, and $j = N/2$. Here, $c_m(t) = \langle j,m|\psi(t)\rangle$ is the corresponding amplitude. Accordingly, the distribution $\{p_m(t)\}$ describes how the evolving state is redistributed over the Dicke-basis components within this totally symmetric subspace.

By tracing out mode b, we acquire the reduced density matrix $\hat{\rho}_a(t)$ of mode a. Due to the conservation of total particle number N, its off-diagonal terms vanish, leading to a diagonal form density matrix, with

$$\hat{\rho}_a(t) = \mathrm{Tr}_b\big[|\psi(t)\rangle\langle\psi(t)|\big] = \sum_{m=-j}^{j} p_m(t)\,|j+m\rangle_{aa}\langle j+m|, \tag{11}$$

where $p_m(t) = |c_m(t)|^2$ denotes the probability distribution. Consequently, the von Neumann entropy of this reduced density matrix reads

$$S_{\mathrm{vN}}(t) = -\mathrm{Tr}\big[\hat{\rho}_a(t)\log\hat{\rho}_a(t)\big] = -\sum_{m=-j}^{j} p_m(t)\log p_m(t), \tag{12}$$

Preprints.org (www.preprints.org) | NOT PEER-REVIEWED | Posted: 31 March 2026 doi:10.20944/preprints202603.2482.v1

where $\log \equiv \log_2$ denotes the logarithm here and throughout. S_{vN} is equivalent to Shannon entropy acquired by counting the probability distribution of Dicke basis in states $|\psi(t)\rangle$. Under the present conditions, this Shannon-form expression is also identical to the mode entanglement entropy $S_{\mathrm{E}}(t)$.

We mention that, for a discrete distribution of dimension $2j+1$, the entropy S_{vN} has a dimension-dependent maximum

$$S_{\mathrm{vN}}^{\max} = \log(2j+1), \tag{13}$$

which is attains when $p_m(t)$ is uniform, i.e., $\{p_m = 1/(2j+1)\}$. Therefore, to remove the dependence of S_{vN} on this dimension, we introduce the normalized Shannon entropy (nSE), with

$$\bar{S}(t) = \frac{S_{\mathrm{vN}}(t)}{S_{\mathrm{vN}}^{\max}} = -\frac{\sum_{m=-j}^{j} p_m(t) \log p_m(t)}{\log(2j+1)}. \tag{14}$$

It takes values in $[0,1]$, with smaller $\bar{S}(t)$ quantifying narrower distributions $\{p_m\}$. Specifically, $\bar{S}(t) \approx 1$ indicates a state approximately uniformly distributed over the Dicke basis, while $S(t) \to 0$ indicates a distribution highly concentrated on a few m components.

It should be emphasized that the equivalence between Eq. (12) and the mode entanglement entropy $S_{\mathrm{E}}(t)$ holds specifically under the conditions assumed here: two modes, fixed total particle number, pure states, and the mode bi-partition $a|b$. It is not valid in general cases. However, $\bar{S}(t)$ is still a valid measure of the dispersion of the probability distribution in the chosen basis.

6. Quantum Dynamics of Normalized Shannon Entropy

In this section, we consider the dynamics of normalized Shannon entropy $\bar{S}(t)$, which serves as a basis-resolved scalar indicator of how concentrated the many-body state is in the Dicke basis.

Firstly, we consider the free evolution with a constant transverse field $\Omega(t) = \Omega_R$ (as depicted by Hamiltonian $\hat{H}_1$). As illustrated in Fig. 3, $\bar{S}(t)$ begins at a relatively high level during the initial stage, reflecting a broad distribution of $\{p_m\}$ over the $\{|j,m\rangle\}$ basis. Under the combined action of OAT and transverse coupling in $\hat{H}_1$, the probability distribution narrows, and $\bar{S}(t)$ decreases rapidly toward its first local minimum that emerges at $t = t_S$. At later times, $\bar{S}(t)$ increases again and exhibits a quasi-periodic oscillatory behavior, consistent with the emergence of many-body interference in the finite-dimensional spin space.

Similar to the dynamics of QFI, switching off the transverse field in the vicinity of the first local minimum of $\bar{S}(t)$ will also convert the transient low-entropy interval into a low-entropy plateau. Specifically, we consider dynamics generated by the Hamiltonian

$$\hat{H}_3(t) = \begin{cases} 2\kappa \hat{J}_z^2 + \Omega_R \hat{J}_x, & 0 \le t \le t_S \\ 2\kappa \hat{J}_z^2, & t_S < t. \end{cases} \tag{15}$$

Here, we set $\Omega(t) = 0$ for $t \ge t_S$, i.e., after $\bar{S}(t)$ reaches its first local minimum under the free evolution generated by $\hat{H}_1$. Fig. 3 presents the effect for different coupling ratios Ω_R/κ. It demonstrates that, for $t \ge t_S$, $S(t)$ remains low and constant, forming a plateau of appreciable duration.

 doi:10.20944/preprints202603.2482.v1

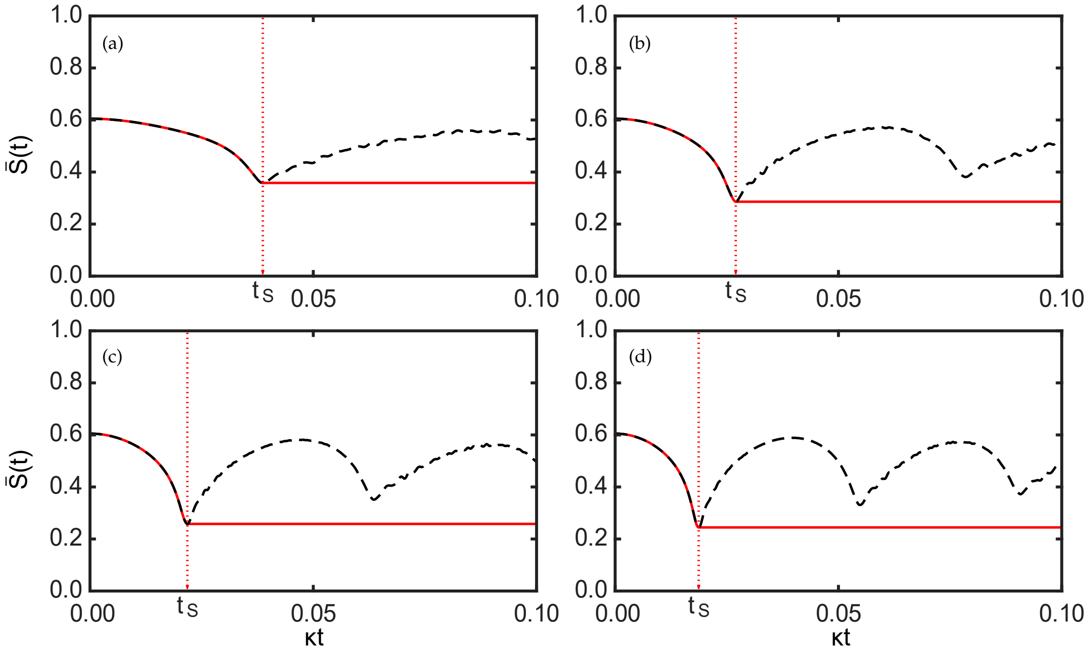

Figure 3. Latching behavior of the normalized Shannon entropy. The total particle number is $N = 1000$. The four panels correspond to (a) $\Omega_R/\kappa = 1$, (b) $\Omega_R/\kappa = 2$, (c) $\Omega_R/\kappa = 3$, and (d) $\Omega_R/\kappa = 4$. The dashed curves show the free-evolution $\bar{S}(t)$. The solid curves show its evolution after switching off the transverse coupling at t_S.

7. Conclusions and Discussions

We have investigated a scheme of generation and stabilization of two quantum-metrological resources: the nQFI $\bar{F}_Q(t)$ serves as the primary precision measure, and the nSE $\bar{S}(t)$ quantifies the degree of concentration of states in the Dicke basis within the fixed-N symmetric collective-spin description. The scheme has been demonstrated by an exemplified two-component BEC system, whose dynamics are governed by the OAT interaction and a controllable transverse coupling, as illustrated by the Hamiltonian Eq. (1).

In the free evolution with a constant transverse field, $\bar{F}_Q(t)$ and $\bar{S}(t)$ display distinct yet correlated temporal structures under the combined action of $\hat{J}_z^2$ and $\hat{J}_x$. In particular, $\bar{F}_Q(t)$ shows a primary peak followed by collapse and quasi-periodic oscillations, whereas $\bar{S}(t)$ exhibits a rapid decrease toward an early-time minimum and then an oscillatory increase. These behaviors also connect the achievable phase sensitivity to the degree of concentration of the state in the Dicke basis.

Based on these observations, we have proposed a free-evolution–switch-off protocol in which the transverse coupling is subsequently switched off at a characteristic time. Two natural choices arise from the free-evolution dynamics, namely, switching off at the first local maximum of $\bar{F}_Q(t)$ at t_F or at the first local minimum of $\bar{S}(t)$ at t_S. The numerical results show that switching off the transverse coupling can convert the transient high-sensitivity or low-entropy intervals into plateaus of appreciable duration in the target metric. This demonstrated that the protocol can robustly stabilize the desired quantum resource—whether it be phase sensitivity or state concentration—thereby extending the usable time window.

In this way, this free-evolution–switch-off protocol can reduce the reliance on the precise control of evolution time and provides a simple and experimentally accessible control rule within the present protocol. This scheme offers a systematic basis for designing time-robust metrological protocols in two-component condensates and for exploring extensions to more general control settings.

Author Contributions: Henan Wang: Software (equal), Writing - original draft (equal); Qimeng Zhang: Validation (equal); Hengyan Wang: Funding acquisition (equal), Supervision (equal); Hai-Jun Xing: Funding acquisition (equal), Writing - review & editing (equal); Yixiao Huang: Funding acquisition (equal), Methodology (equal), Supervision (equal), Writing - review & editing (equal). All authors have read and agreed to the published version of the manuscript.

Funding: This work was supported by the Natural Science Foundation of Zhejiang Province under Grant No. LY24A050005, the Fundamental Research Funds for the Zhejiang University of Science and Technology under Grant No. 2023JLZD010, and the Fundamental Research Funds for the Central Universities (Grant No. 2412023QD007).

Data Availability Statement: The data that support the findings of this study are available from the corresponding author upon reasonable request.

Conflicts of Interest: The authors declare no conflicts of interest.

References

1. Helstrom, C.W. *Quantum detection and estimation theory*; Vol. 123, *Mathematics in Science and Engineering*, Academic Press: New York, 1976.
2. Holevo, A.S. *Probabilistic and statistical aspects of quantum theory*; Vol. 1, Springer, 2011. https://doi.org/10.1007/978-88-7642-378-9.
3. Caves, C.M. Quantum-mechanical noise in an interferometer. *Phys. Rev. D* **1981**, *23*, 1693–1708. https://doi.org/10.1103/PhysRevD.23.1693.
4. Wineland, D.J.; Bollinger, J.J.; Itano, W.M.; Moore, F.L.; Heinzen, D.J. Spin squeezing and reduced quantum noise in spectroscopy. *Phys. Rev. A* **1992**, *46*, R6797–R6800. https://doi.org/10.1103/PhysRevA.46.R6797.
5. Kitagawa, M.; Ueda, M. Squeezed spin states. *Phys. Rev. A* **1993**, *47*, 5138–5152. https://doi.org/10.1103/PhysRevA.47.5138.
6. Giovannetti, V.; Lloyd, S.; Maccone, L. Quantum metrology. *Phys. Rev. Lett.* **2006**, *96*, 010401. https://doi.org/10.1103/PhysRevLett.96.010401.
7. Ma, J.; Wang, X.; Sun, C.P.; Nori, F. Quantum spin squeezing. *Phys. Rep.* **2011**, *509*, 89–165. https://doi.org/10.1016/j.physrep.2011.08.003.
8. Huang, J.; Zhuang, M.; Lee, C. Entanglement-enhanced quantum metrology: From standard quantum limit to Heisenberg limit. *Appl. Phys. Rev.* **2024**, *11*, 031302. https://doi.org/10.1063/5.0204102.
9. Cronin, A.D.; Schmiedmayer, J.; Pritchard, D.E. Optics and interferometry with atoms and molecules. *Rev. Mod. Phys.* **2009**, *81*, 1051–1129. https://doi.org/10.1103/RevModPhys.81.1051.
10. Pezzè, L.; Smerzi, A.; Oberthaler, M.K.; Schmied, R.; Treutlein, P. Quantum metrology with nonclassical states of atomic ensembles. *Rev. Mod. Phys.* **2018**, *90*, 035005. https://doi.org/10.1103/RevModPhys.90.035005.
11. Sørensen, A.; Duan, L.M.; Cirac, J.I.; Zoller, P. Many-particle entanglement with Bose-Einstein condensates. *Nature* **2001**, *409*, 63–66. https://doi.org/10.1038/35051038.
12. Jin, G.R.; Kim, S.W. Storage of spin squeezing in a two-component Bose-Einstein condensate. *Phys. Rev. Lett.* **2007**, *99*, 170405. https://doi.org/10.1103/PhysRevLett.99.170405.
13. Estève, J.; Gross, C.; Weller, A.; Giovanazzi, S.; Oberthaler, M.K. Squeezing and entanglement in a Bose-Einstein condensate. *Nature* **2008**, *455*, 1216–1219. https://doi.org/10.1038/nature07332.
14. Gross, C. Spin squeezing, entanglement and quantum metrology with Bose-Einstein condensates. *J. Phys. B: At. Mol. Opt. Phys.* **2012**, *45*, 103001. https://doi.org/10.1088/0953-4075/45/10/103001.
15. Milburn, G.J.; Corney, J.; Wright, E.M.; Walls, D.F. Quantum dynamics of an atomic Bose-Einstein condensate in a double-well potential. *Phys. Rev. A* **1997**, *55*, 4318–4324. https://doi.org/10.1103/PhysRevA.55.4318.
16. Silva, R.E.F.; Feist, J. Permutational symmetry for identical multilevel systems: A second-quantized approach. *Phys. Rev. A* **2022**, *105*, 043704. https://doi.org/10.1103/PhysRevA.105.043704.
17. Steel, M.J.; Collett, M.J. Quantum state of two trapped Bose-Einstein condensates with a Josephson coupling. *Phys. Rev. A* **1998**, *57*, 2920–2930. https://doi.org/10.1103/PhysRevA.57.2920.
18. Law, C.K.; Ng, H.T.; Leung, P.T. Coherent control of spin squeezing. *Phys. Rev. A* **2001**, *63*, 055601. https://doi.org/10.1103/PhysRevA.63.055601.
19. Smerzi, A.; Fantoni, S.; Giovanazzi, S.; Shenoy, S.R. Quantum coherent atomic tunneling between two trapped Bose-Einstein condensates. *Phys. Rev. Lett.* **1997**, *79*, 4950–4953. https://doi.org/10.1103/PhysRevLett.79.4950.
20. Albiez, M.; Gati, R.; Fölling, J.; Hunsmann, S.; Cristiani, M.; Oberthaler, M.K. Direct observation of tunneling and nonlinear self-trapping in a single bosonic Josephson junction. *Phys. Rev. Lett.* **2005**, *95*, 010402. https://doi.org/10.1103/PhysRevLett.95.010402.
21. Gati, R.; Oberthaler, M.K. A bosonic Josephson junction. *J. Phys. B: At. Mol. Opt. Phys.* **2007**, *40*, R61. https://doi.org/10.1088/0953-4075/40/10/R01.

22. Gross, C.; Zibold, T.; Nicklas, E.; Esteve, J.; Oberthaler, M.K. Nonlinear atom interferometer surpasses classical precision limit. *Nature* **2010**, *464*, 1165–1169. https://doi.org/10.1038/nature08919.
23. Riedel, M.F.; Böhi, P.; Li, Y.; Hänsch, T.W.; Sinatra, A.; Treutlein, P. Atom-chip-based generation of entanglement for quantum metrology. *Nature* **2010**, *464*, 1170–1173. https://doi.org/10.1038/nature08988.
24. Lücke, B.; Scherer, M.; Kruse, J.; Pezzè, L.; Deuretzbacher, F.; Hyllus, P.; Topic, O.; Peise, J.; Ertmer, W.; Arlt, J.; et al. Twin matter waves for interferometry beyond the classical limit. *Science* **2011**, *334*, 773–776. https://doi.org/10.1126/science.1208798.
25. Ockeloen, C.F.; Schmied, R.; Riedel, M.F.; Treutlein, P. Quantum metrology with a scanning probe atom interferometer. *Phys. Rev. Lett.* **2013**, *111*, 143001. https://doi.org/10.1103/PhysRevLett.111.143001.
26. Dicke, R.H. Coherence in spontaneous radiation processes. *Phys. Rev.* **1954**, *93*, 99–110. https://doi.org/10.1103/PhysRev.93.99.
27. Shannon, C.E. A mathematical theory of communication. *Bell Syst. Tech. J.* **1948**, *27*, 379–423. https://doi.org/10.1002/j.1538-7305.1948.tb01338.x.
28. Tóth, G.; Apellaniz, I. Quantum metrology from a quantum information science perspective. *J. Phys. A: Math. Theor.* **2014**, *47*, 424006. https://doi.org/10.1088/1751-8113/47/42/424006.
29. Coles, P.J.; Berta, M.; Tomamichel, M.; Wehner, S. Entropic uncertainty relations and their applications. *Rev. Mod. Phys.* **2017**, *89*, 015002. https://doi.org/10.1103/RevModPhys.89.015002.
30. Law, C.K.; Pu, H.; Bigelow, N.P. Quantum spins mixing in spinor Bose-Einstein condensates. *Phys. Rev. Lett.* **1998**, *81*, 5257–5261. https://doi.org/10.1103/PhysRevLett.81.5257.
31. Williams, J.; Walser, R.; Cooper, J.; Cornell, E.; Holland, M. Nonlinear Josephson-type oscillations of a driven, two-component Bose-Einstein condensate. *Phys. Rev. A* **1999**, *59*, R31–R34. https://doi.org/10.1103/PhysRevA.59.R31.
32. Huang, Y.; Zhang, Y.; Lü, R.; Wang, X.; Yi, S. Macroscopic quantum coherence in spinor condensates confined in an anisotropic potential. *Phys. Rev. A* **2012**, *86*, 043625. https://doi.org/10.1103/PhysRevA.86.043625.
33. Sinatra, A.; Castin, Y. Binary mixtures of Bose-Einstein condensates: Phase dynamics and spatial dynamics. *Eur. Phys. J. D* **2000**, *8*, 319–332. https://doi.org/10.1007/s100530050042.
34. Huang, J.; Wu, S.; Zhong, H.; Lee, C. Quantum metrology with cold atoms. *Annu. Rev. Cold At. Mol.* **2014**, *2*, 365–415. https://doi.org/10.1142/9789814590174_0007.
35. Chin, C.; Grimm, R.; Julienne, P.; Tiesinga, E. Feshbach resonances in ultracold gases. *Rev. Mod. Phys.* **2010**, *82*, 1225–1286. https://doi.org/10.1103/RevModPhys.82.1225.
36. Braunstein, S.L.; Caves, C.M. Statistical distance and the geometry of quantum states. *Phys. Rev. Lett.* **1994**, *72*, 3439–3443. https://doi.org/10.1103/PhysRevLett.72.3439.
37. Amico, L.; Fazio, R.; Osterloh, A.; Vedral, V. Entanglement in many-body systems. *Rev. Mod. Phys.* **2008**, *80*, 517–576. https://doi.org/10.1103/RevModPhys.80.517.